Photogating-driven enhanced responsivity in few-layered ReSe2 phototransistor

ARTICLE

Photogating-driven enhanced responsivity in few-layered ReSe₂ phototransistor

Prasanna D. Patil,[a] Milinda Wasala,[a†] Rana Alkhaldi,[a] Lincoln Weber,[a] Kiran Kumar Kovi,[b] Bhaswar Chakrabarti,[b,c] Jawnaye A. Nash,[d] Daniel Rhodes,[e] Daniel Rosenmann,[b] Ralu Divan,[b] Anirudha V. Sumant,[b] Luis Balicas,[e] Nihar Pradhan[b,d,e,*] and Saikat Talapatra[a,*]

A wide variety of two-dimensional (2D) metal dichalcogenide compounds have recently attracted much research interest due to their very high photoresponsivies (R) making them excellent candidates for optoelectronic applications. High R in 2D photoconductors is associated to trap state dynamics leading to a photogating effect, which is often manifested by a fractional power dependence (γ) of the photocurrent (I_{ph}) when under an effective illumination intensity (P_{eff}). Here we present photoconductivity studies as a function of gate voltages, over a wide temperature range (20 K to 300 K) of field-effect transistors fabricated using thin layers of mechanically exfoliated rhenium diselenide (ReSe₂). We obtain very high responsivities R ~ 16500 A/W and external quantum efficiency (EQE) ~ 3.2 x 10⁶ % (at 140 K, V_g = 60 V and P_{eff} = 0.2 nW). A strong correlation between R and γ was established by investigating the dependence of these two quantities at various gate voltages and over a wide range of temperature. Such correlations indicate the importance of trap state mediated photogating and its role in promoting high photo responsivities in these materials. We believe such correlations can offer valuable insights for the design and development of high performance photoactive devices using 2D materials.

Introduction

Two-dimensional (2D) layered semiconducting materials are becoming a primary focus of scientific research due to the optical properties resulting from their unique structures, flat geometry, high charge carrier mobility, tunable bandgaps, optical sensitivity etc.[1-8] Photoconduction is one of the most studied properties of these 2D materials due to the layered dependent tunable band structure, which is suitable for photodetection and hence can lead to the development of high performance photodetectors and/or other optoelectronic components such as phototransistors.[1-4] The inherent presence of trap states in these 2D/low dimensional materials and/or traps at the interface (formed between these materials and their supporting substrates) play a crucial role in determining their photoconductive properties. The optical performance of these materials can be tailored and optimized by studying the dynamics of these trap states under illumination.[1] Indeed a large number of studies indicate that trap dominated optical

processes can lead to photodetectors with high responsivities and detectivities.[1, 2, 5, 9-13] A key consequence of trap states in these systems is photogating, a phenomenon in which the conductivity of a phototransistor device is modulated by light-induced gate-like electric field or local gating.[1, 2] Many recent studies,[1, 2, 9] suggest that the gate-like electric field is primarily produced by the photo-generated charge carries occupying the traps states. However, this is not the only way a device can experience photogating effect.[1] In the case of carbon nanotube[14] and graphene[15] field effect transistors (FETs), it has been shown that the absorption of a photon by the underlying silicon can generate an electron-hole pair. These light generated carriers can separate and accumulate at the Si/SiO₂ interface due to the presence of a build-in field, giving rise to a photovoltage, thus acting as an additional gate (or interfacial gate), which can significantly enhance the gain of a photodetector.

In a photo-FET based photodetector, the primary manifestation of photogating is associated with the fractional power dependence of the photocurrent (I_{ph}) on the illumination intensity (P).[1] In other words, $I_{ph} \sim P^{\gamma}$ with 0 < γ < 1. Such dependence is quite common in a variety of recently investigated 2D-based photodetectors / phototransistors.[9-12] Specifically, such fractional values of the power exponent γ, coupled with the exceptional values of the photo-responsivities have been observed in phototransistors fabricated using several selenide based 2D layered materials, such as MoSe₂,[16] WSe₂,[11] InSe,[17] In₂Se₃,[9] CuIn₇Se₁₁,[10] etc. These studies indicate that the values of the power exponent γ, as well as its variation under the influence of external parameters such as back gate voltage,

a. *Department of Physics, Southern Illinois University Carbondale IL-62901, USA. Email: saikat@siu.edu.*
b. *Center for Nanoscale Materials, Argonne National Laboratory, Argonne, IL-60439, USA.*
c. *Institute for Molecular Engineering, University of Chicago, IL- 60637, USA.*
d. *Department of Chemistry, Physics and Atmospheric Science, Jackson State University, Jackson, MS-39217, USA. Email: nihar.r.pradhan@jsums.edu.*
e. *National High Magnetic Field Laboratory, Tallahassee, FL-32310, USA.*
† Present Address: Science Department, Great Basin College, Elko, NV 89801, USA.
Electronic Supplementary Information (ESI) available: Estimation of contact resistance: γ-function method, External quantum efficiency (EQE), Electronic and optoelectronic transport of device 2. See DOI: 10.1039/x0xx00000x

temperature etc. can provide insight into the extent of photogating under several conditions and its influence on the responsivities of phototransistor devices. In this work we show how photogating is responsible for the high responsivity of ReSe$_2$ based photo-FET.

Re-based TMDs have attracted attention due to their unique in-plane anisotropic transport properties.[12, 18-23] ReSe$_2$ is an indirect bandgap material[24] (bandgap of 1.27 eV for bulk and 1.24 eV for a monolayer) that shows anisotropic electrical and optical properties.[24] In our study, the FET devices we measured show a clear non-monotonic variation of the photo-responsivities and photogating with decreasing temperature. A very strong correlation between the variation of the power exponent (as a function of the temperature) and the photo-responsivities emerges, which strongly suggests the role of trap states in driving the mechanism of photoconduction in these devices from purely photoconductive to photogating.

Results and discussions

ReSe$_2$ has unique distorted 1T-phase crystal structure, unlike other 2H-phase TMDs, as shown in Figure 1a which exhibits unique in-plane anisotropic transport properties for electrical currents flowing along the a and b axis.

The experimental section contains a detailed description of the growth of ReSe$_2$ single crystals and the fabrication of ReSe$_2$ devices. Figure 1b shows an optical image of one of the ReSe$_2$ phototransistor devices fabricated on a 285 nm thick SiO$_2$ film deposited on a highly p-doped Si substrate. All the electrical and

Figure 1. Structure of ReSe$_2$ and characterization of FET device. a) Structure of ReSe$_2$ along the a-, b- and c-axis with 6.8 Å being the thickness of the monolayer. b) Optical microscope image of the ReS$_2$ device presented in this manuscript. c) Atomic force microscope (AFM) height profile of a ReSe$_2$ flake taken along the red line shown in (b). ReSe$_2$ flake height was estimated to be ~ 7.5 nm which correspond to ~ 11 layers.

optical transport measurements were performed using S and D contacts corresponding to source and drain terminals, respectively. An AFM height profile taken along the red line in Figure 1b is shown in Figure 1c. The estimated flake thickness of the device is 7.5 nm, which corresponds to 11 layers assuming a monolayer thickness of ~ 0.7 nm.[20]

ReSe$_2$ FET: Electronic transport

Electronic transport measurements, shown in Figure 2, were performed on a ReSe$_2$ FET using SiO$_2$ as a back gate. Figure 2a depicts the room temperature FET transport characterization of a few layered ReSe$_2$ device measured at room temperature, showing drain current (I_d) as a function of the applied gate voltage (V_g) at constant drain voltage $V_d = 0.2$V, commonly known as the transfer characteristics. The blue curve depicts the I_d-V_g characteristics in semi-log scale while the red curve represents the characteristics in linear scale. The conduction is found to be following predominantly *n*-type behavior, which indicates electrons to be the majority charge carriers in ReSe$_2$ channel. We found a signature for *p*-type transport for $V_g < -35$ V indicating ambipolar behavior in ReSe$_2$ where holes constitute the dominant charge carriers.[22, 25] However, the observed hole current is almost 3 orders of magnitude smaller than the electron current indicating an electron-rich ReSe$_2$ channel. Similar ambipolar behavior with high electron mobility compared to hole is also reported for a few-layered ReSe$_2$ FET [22]. As V_g increases from -60 V to 60 V, the ReSe$_2$ channel starts conducting for gate voltages (known as V_{on}) greater than -30 V due to electrostatic doping. The FET is known to be in the on-state for $V_g > V_{on}$. Maximum on-state current ($I_{d,on}$) is found to be 7.45×10^{-6} A at $V_g = 60$ V. The FET remains in the off-state for $V_g < V_{on}$ and the minimum off-state current ($I_{d,off}$) was found to be ~ 0.19×10^{-10} A. The current on/off ratio for this particular FET was measured to be ~ 10^3.

Subthreshold swing (SS), is defined as the gate voltage required to increase the drain current by an order of magnitude in the subthreshold region, can be mathematically determined through Equation 1,[26, 27]

$$SS = \left(\left| \frac{\partial \, log(I_d)}{\partial V_g} \right|_{max} \right)^{-1} \tag{1}$$

We found the SS value of ~ 6.1 V/dec, estimated from the slope of the transfer curve (semi-log scale) in the subthreshold region (denoted by orange line in Figure 2a). Deviation from the ideal SS (~ 60 mV/dec at T = 300 K) is often found in various 2D-materials based FETs[28-30] and it can be ascribed to a depletion layer formed by mid-gap states (commonly known as localized or trap states).[26] The origin of these trap states in ReSe$_2$ FET devices, like in many other reported 2D FET's, is unknown. However it is generally believed that trap states commonly arise due to structural defects in channel and/or due to vacancies, like in the case of missing chalcogen atoms.[31] Charge traps also arise at the interface between the channel materials and SiO$_2$, due to the presence of dangling bonds in SiO$_2$.[32] The inherent presence of trap states in semiconducting devices plays a significant role in their overall operation, as charge carriers can
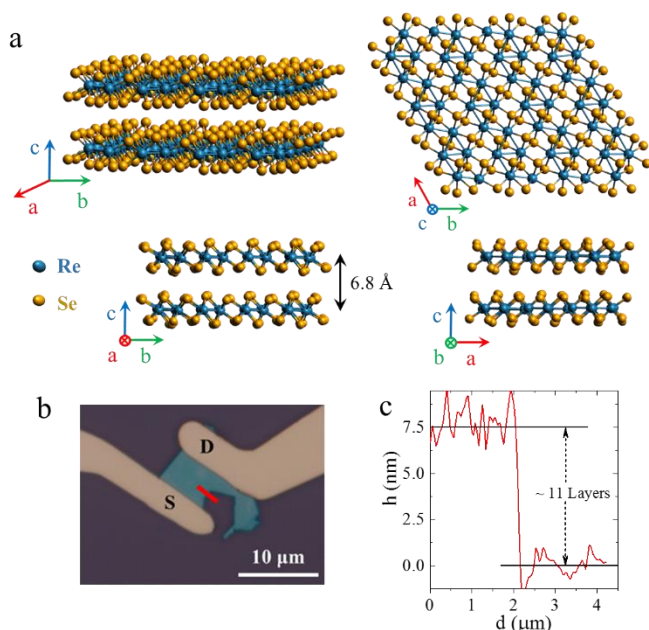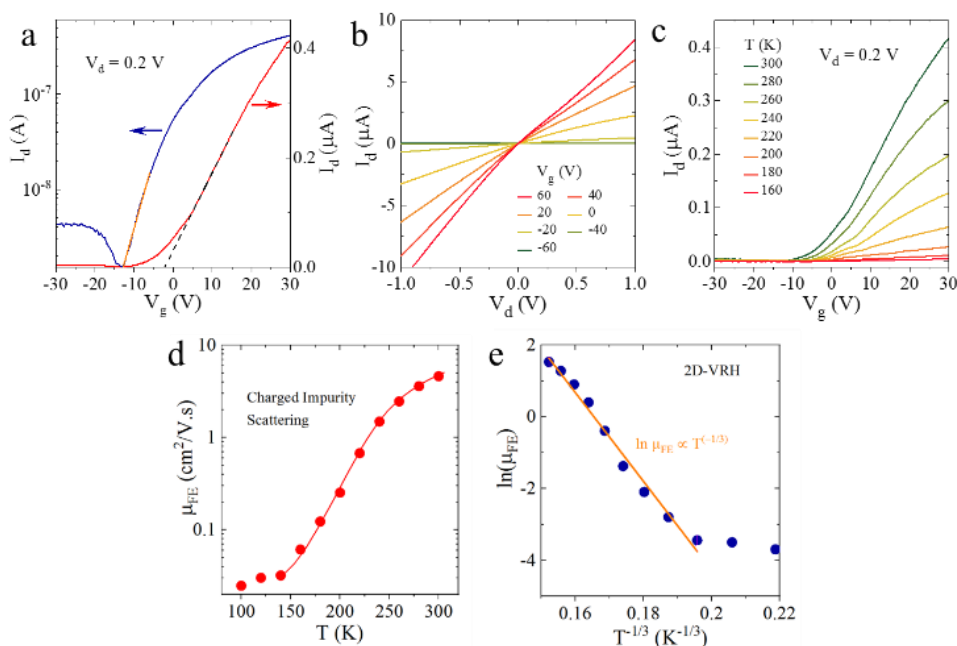
ARTICLE

Figure 2. Electronic transport of ReSe$_2$ FET. a) Transfer characteristics (I_d *vs* V_g) at V_d = 0.2V, in a linear scale (red) and in a semi-log scale (blue). Black dashed and orange lines indicate a region of the curve utilized to calculate the field-effect mobility (μ_{FE}) and the subthreshold swing (SS) respectively. b) Output characteristics (I_d *vs* V_d) under different applied gate voltages (-60 V < V_g < 60 V). c) Temperature dependent (100 K < T < 300 K) transfer characteristics curves under V_d = 0.2 V. d) Dependence of the field-effect mobility (μ_{FE}) as a function of the temperature. e) A plot in ln(μ_{FE}) *vs* T$^{-1/3}$ along with fitting of ln(μ_{FE}) $\propto$ T$^{-1/3}$ (orange lines) indicating the possibility of electron transport dominated by 2D-variable range hopping.[32]

be trapped in these states and become localized. Although charge carriers can become free either by absorbing the energy needed to escape (usually thermal or light), by tunnelling through the trap barrier or by hopping from one trap to another.

The Density of trap states (N_{tr}) can be estimated from SS (equation 1) by using the formula (equation 2),[26, 33]

$$SS = \ln(10)\frac{kT}{e}\left(1 + \frac{e^2 N_{tr}}{C_{ox}}\right) \qquad (2)$$

where, e is the electronic charge, k is the Boltzmann constant and C_{ox} is an oxide capacitance. Here C_{ox} = 1.16 × 10^{-8} F/cm^2, is the capacitance per unit area of 285 nm thick SiO$_2$ dielectric. For our ReSe$_2$ device shown in Figure 2, N_{tr} ~ 7.3 × 10^{12} cm^{-2} eV^{-1}. For SiO$_2$ substrate, a typical value of N_{tr} is of the order of 10^{12} cm^{-2} eV^{-1}. We would like to note that, in case of other 2D materials based devices such as black phosphorous,[34] subthreshold swing (SS) has a relatively constant value at low source drain voltage (|V_d|) and this constant value of SS is limited by trap states and not the contact resistance. At higher V_d, SS values increases due to electron back-injection from the drain,[34] in other words contact resistance. For our ReSe$_2$ device, SS value of ~ 6.1 V/dec was extracted at V_d = 0.2 V. Since V_d is low, we believe that SS is limited by trap states and contact resistance is minimal effect on SS. Thus extracted density of trap states (N_{tr} ~ 7.3 × 10^{12} cm^{-2} eV^{-1}) is reasonable.

One of the key performance parameters of an FET, the field-effect mobility (μ_{FE}), is defined as the average drift speed of

charge carries under an unit of electric field, which can be estimated using the formula shown in Equation 3,

$$\mu_{FE} = \frac{L}{W\,C_{ox}\,V_d}\frac{\partial I_d}{\partial V_g} \qquad (3)$$

For our ReSe$_2$ device, the channel length L ≈ 4.5 µm, width W ≈ 6 µm (Figure 1 (b)) and the maximum transconductance (g_m = $\partial I_d/\partial V_g$) was found to be between 10 V < V_g < 30 V. From these values we estimated the field effect charge carrier mobility as μ_{FE} ~ 4.6 cm^2 V^{-1} s^{-1}. This value of μ_{FE} is either comparable to or slightly lower than μ_{FE} of selenide-based FETs.[5] The mobility of a FET can depend upon several internal factors such as disorder potential, distribution of trap states, barrier at metal-semiconductor junction *etc.* and external factors such as temperature, electric field *etc.*[35, 36] We would like to note here that the measurements presented in this article are based on 2-terminal geometry and hence it is important to estimate the contact resistances of our devices. The contact resistance (R_C) of our devices were estimated by Y-function method[37, 38] and was found to be ~ 773 KΩ which is significantly lower than the minimum channel resistance at V_g = 30 V (details are shown in Supporting Information, Figure S1 and S2). Output characteristics (I_d *vs* V_d) measured under different applied gate voltages (- 60 V < V_g < 60 V) are shown in Figure 2b. The linear nature of the output characteristics curves could be reasoned to the channel dominated conduction through the device. The effect of contact resistance in the device is perhaps minimal. This is further evident from the comparison of the temperature
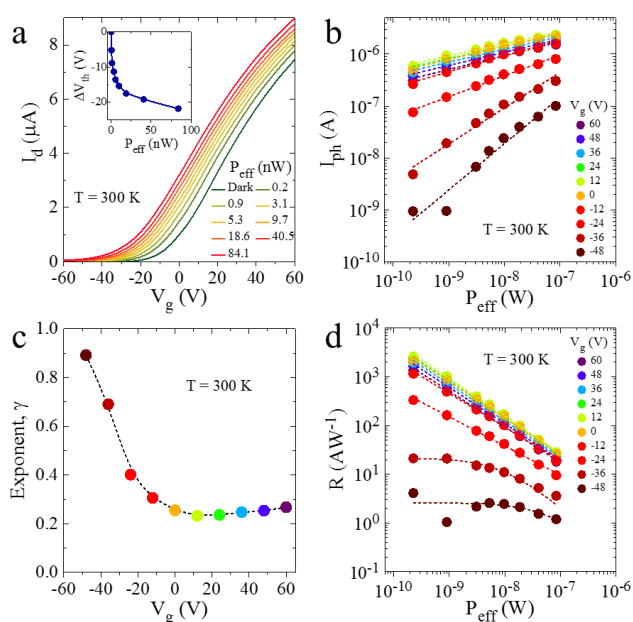
Figure 3. Optoelectronic transport of a ReSe$_2$ phototransistor at room temperature (300 K). a) Transfer characteristics (I$_d$ vs V$_g$) at V$_d$ = 1V under laser illumination (λ = 640 nm) with different effective laser intensities (0.2 nW < P$_{eff}$ < 84.1 nW). b) Photocurrent (I$_{ph}$) as a function of the effective laser intensity (P$_{eff}$) under different applied gate voltages (-48 V < V$_g$ < 60 V). Straight dashed line indicates a fitting to I$_{ph} \propto$ (P$_{eff}$)$^\gamma$. c) Variation of the power exponent (γ) as a function of the applied gate voltage (V$_g$). d) Responsivity (R) as a function of the effective laser intensity (P$_{eff}$) under different applied gate voltages (-48 V < V$_g$ < 60 V). Dashed line indicates fitting of either R $\propto$ (P$_{eff}$)$^{(\gamma-1)}$ [1] or R = A$_1$/(A$_2$ + P$_{eff}$).[39]

Figure 4. Optoelectronic transport of a ReSe$_2$ phototransistor at the low temperature (T = 140 K). a) Transfer characteristics (I$_d$ vs V$_g$) at V$_d$ = 1V under laser illumination (λ = 640 nm) with different effective intensities (0.2 nW < P$_{eff}$ < 84.1 nW). b) Photocurrent (I$_{ph}$) as a function of the effective laser intensity (P$_{eff}$) under different applied gate voltages (-36 V < V$_g$ < 60 V). Straight dashed lines indicate fittings to I$_{ph} \propto$ (P$_{eff}$)$^\gamma$. c) Variation of the power exponent (γ) as a function of applied gate voltage (V$_g$). d) Responsivity (R) as a function of the effective laser intensity (P$_{eff}$) under different the applied gate voltages (-36 V < V$_g$ < 60 V). Dashed lines indicate fittings to either R $\propto$ (P$_{eff}$)$^{(\gamma-1)}$ [1] or R = A$_1$/(A$_2$ + P$_{eff}$).[39]

dependence of contact resistance, RC with respect to the channel resistance (details in Supplementary Information, Figure S1).

Transfer characteristics at lower temperature (160 K < T < 300 K) at V$_d$ = 0.2 V are shown in Figure 2c. For the entire temperature range shown, FET characteristic follows predominantly *n*-type conduction and we found that the channel current decreases as a function of decreasing temperature (Figure 2c), which is a typical semiconductor characteristic. At room temperature electron hopping through traps plays an important role in moving the majority of charge carriers through the potential barrier within the semiconducting channel. In addition, with decrease in temperature hoping decreases thus restricting the movement of the charge carriers through the channel and therefore the conduction is expected to decrease.

The variation of μ_{FE} as a function of temperature is shown in Figure 2d. One can observe that in general the mobility value decreases with decreasing temperature (from 4.6 cm^2 V^{-1} s^{-1} at 300 K to 0.02 cm^2 V^{-1} s^{-1} at 100 K) which constitutes a typical behaviour of mobilities where conduction is mainly limited by charge-impurity scattering.[35, 40] Electron mobility in transistors is affected by several scattering mechanisms and, even in state-of-the-art transistors, experimental mobility is found to be
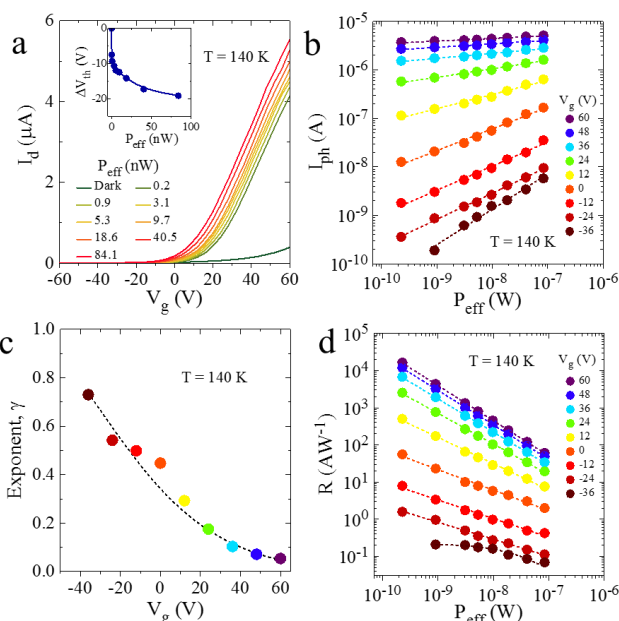
significantly lower than that in phonon-limited mobility (theoretically predicted upper limit) [35]. The presence of charge traps / localized states, Coulomb impurities at channel-substrate interface, defects in channel, and surface optical phonons (interaction with optical phonons in dielectric) could lead to charge-impurity scattering.[35] In the presence of traps states, electrons find a conduction path *via* hopping between these traps states as predicted by Mott[41]. Mott's variable-range hopping (VRH) gives a theoretical description of conduction in a strong disordered system[41]. We analysed the charge carrier mobility as a function of the temperature using the VRH model. For VRH in two-dimensions, the temperature dependence of the mobility should follow ln $\mu \propto$ T$^{-1/(d+1)}$, with d=2 being the dimensionality of the charge transport.[28, 32] Figure 2e shows a plot of ln μ_{FE} as a function of T$^{-1/3}$ where the fitting (orange line) corresponds to ln $\mu \propto$ T$^{-1/3}$. This suggests that the electron transport in ReSe$_2$ is dominated by traps or disorders within the channel, with a strong indication of 2D-VRH.

ReSe$_2$ FET: Optoelectronic transport

The optoelectronic properties of ReSe$_2$ FETs were investigated using a continuous wave laser with illumination wavelength λ = 640 nm (E = 1.94 eV) and a spot size of ~ 3 mm in diameter. The
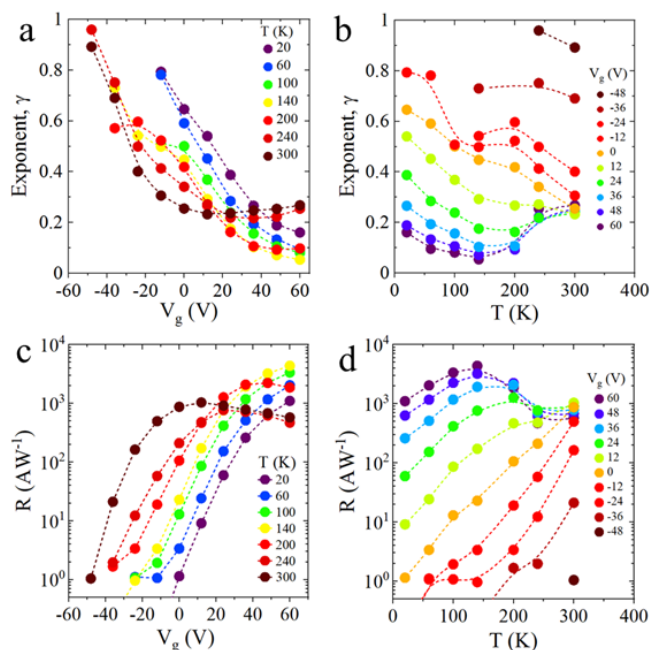
Figure 5. Power exponent (γ) and responsivity (R) as a function of the applied gate voltage (V_g) and temperature (T). a) Exponent (γ) as a function of the applied gate voltage (V_g) under different temperatures (20 K < T < 300 K). b) Power exponent (γ) as a function of the temperature (T) under different applied gate voltages (-48 V < V_g < 60 V). c) Responsivity (R) as a function of applied gate voltage (V_g) under different temperatures (60 K < T < 300 K). d) Responsivity (R) as a function of the temperature (T) under different applied gate voltages (-48 V < V_g < 60 V).

spot size used was large compared to our device dimensions. Larger laser spot size compared to the device dimensions leads to the uniform illumination of optical power on the channel of the device as well as on both contacts. Under the condition that both contacts receive similar amounts of laser illumination, it can be assumed that the contribution from thermal effects such as the photo-thermoelectric effect and photo-bolometric effect *etc.* can be neglected[9]. Owing to the smaller size of the device compared to the laser spot, laser intensity (P_{laser}) was scaled to an effective laser intensity (P_{eff}) per unit area of device (A_{device}) and the area of laser spot (A_{spot}) given by $P_{eff} = P_{laser} \times A_{device}/A_{spot}$.

The optoelectronic transport measurements of a ReSe$_2$ FET at room temperature (300 K) is shown in Figure 3. The transfer characteristics under different effective laser intensities (0.2 nW < P_{eff} < 84.1 nW) at $V_d = 1$ V are shown in Figure 3a. Several observations can be made from the data shown in Figure 3a. First, upon laser illumination, the drain current (I_d) increases with a laser intensities used throughout the gate voltage sweep window as evidenced by the vertical shift of the transfer characteristics curves in Figure 3a. Second, there is a shift in the threshold voltage with increasing laser power. The vertical shift of the transfer characterization is attributed to electron-hole pair generation by incident photons, commonly known as photoconduction or photoconductive effect.[2] The horizontal shift indicates the effect of trap states present in the device [2, 9, 10]. In the presence of trap states, the minority charge carrier gets trapped, resulting in a delay of the recombination of

electron-hole pair, thus prolonging the minority carrier lifetime. These trapped charges can, as a result, produce a local electric field similar to the applied gate voltage, hence modulating the channel conductance. This effect is known as photogating. [1, 2]. Photogating was observed in our devices, as seen in Figure 3a. Trapping of charge carries will lead to a shift in the threshold voltage ($\Delta V_{th} = V_{th,illuminated} - V_{th/dark}$) and ΔV_{th} as a function of P_{eff} is shown in the inset of Figure 3a. In a predominately *n*-type channel, the minority charge carriers (holes) can act as trap states and when trap states are opposite to that of majority charge carriers (electrons), a positive photocurrent can be obtained along with a shift of V_{th} to negative V_g ($\Delta V_{th} < 0$).[1] Photoconductive as well as photogating dominated photo response has been observed in various 2D-based phototransistors.[1, 2, 9-12, 42, 43]

The photocurrent produced by local gating (photo-gating) can be written as $I_{ph} = g_m \times \Delta V_g$, where the transconductance (g_m) depends on the mobility of the channel and ΔV_g is a local gate voltage. The photo generated local gating could originate from either interfacial gating or trap-induced gating. The interfacial gating arises from photo-induced charge carriers produced in the underlying Si and their subsequent accumulation at the SiO$_2$/Si interface. Trap-induced gating originates from the trapping of photo-induced minority carriers at defect/trap states within the semiconducting channel. It should be noted that MoS$_2$ devices did not show interfacial gate effect and it is reasoned to lower mobility (0.1-10 cm^2 V^{-1} s^{-1}) of device, compared to that of graphene.[15] In addition, SiO$_2$/Si interfacial gating induces a negative photo-voltage.[1] In photoactive materials such as MoS$_2$ the combination of low mobility and negative photo-voltage will lead to a negligible effect of interfacial gating on photocurrent.[1] Few-layered ReSe$_2$ exhibits a low mobility (8.5 cm^2 V^{-1} s^{-1}), compared to that of graphene,[15] thus interfacial gating should play an insignificant role in photogating. However, trap states, evident from the SS, could be the source of photogating in ReSe$_2$ FETs. When the channel is illuminated by light, photogenerated holes are captured at trap states and, as a consequence, trapping prolongs the electron-hole recombination times thus enhancing the gain.

The photocurrent ($I_{ph} = I_{illuminated} - I_{dark}$) was extracted at different applied gate voltages (-48 V < V_g < 60 V) and is plotted as a function P_{eff} in log-log scale in Figure 3b. The photocurrent follows a power law dependence with respect to the effective laser power as $I_{ph} \propto (P_{eff})^\gamma$ where the value of the exponenet (γ) is $0 \leq \gamma \leq 1$. Power law fits are shown as dashed lines in Figure 3b. Estimated values of the exponenet, γ from Figure 3(b) as a function of gate voltages are shown in Figure 3c. In the case of pure photoconduction, γ will have a value close to 1 (γ = 1), however in photogating, due to other various processes such as trapping and carrier generation / recombination, the exponenet becomes fractional (γ < 1).[1, 2] For $V_g = -48$ V, γ ~ 0.90 which is close to 1 and may be attributed to a photoconductive effect. As gate voltages increase from negative to positive or when the transistor goes from off-state to on-state, γ decreases to a value of ~ 0.25 at $V_g \geq 0$ V indicating the presence of the photogating effect. A crossover of photoconducting mechanism from
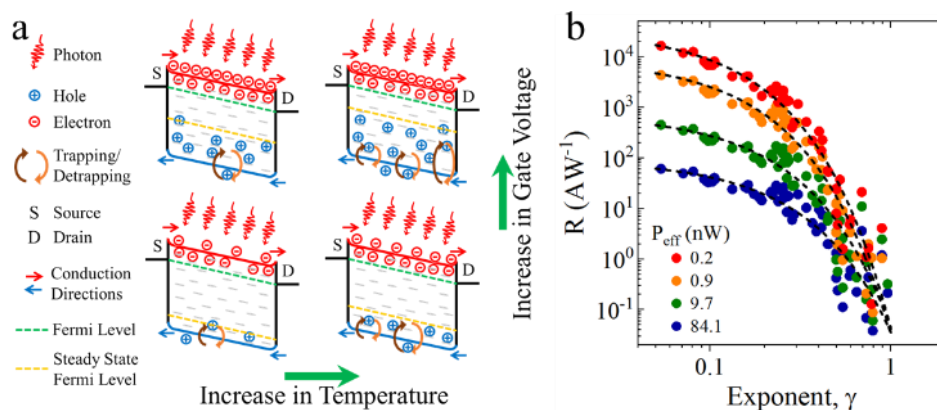
Figure 6. a) Schematic of modulation of trapping/detrapping of minority carriers and movement of steady state Fermi level (yellow dashed line) as a function of change in temperature and gate voltages. b) Responsivity (R) as a function of power exponent (γ) in the temperature range (20 K < T < 300 K) and applied gate voltages (-48 V < V_g < 60 V). Dashed line is a guide to the eye.

photoconductive to photogating as a result of the applied gate voltage has been observed in 2D materials such as In_2Se_3,[9] $CuIn_7Se_{11}$,[10] and recently in ReS_2[12].

Further, we extracted the photo-responsivity (commonly known as responsivity) of a phototransistor, which is defined as the ratio of the photocurrent generated to the effective laser illumination intensity, $R = I_{ph} / P_{eff}$. The responsivity as a function of P_{eff} in log-log scale for several applied gate voltages (-48 V < Vg < 60 V) is shown in Figure 3d. In the case of a photoconduction dominated photocurrent where photoconductive gain is absent, responsivity will have an upper limit given by $R = (η × e × λ) / (h × c) = η × λ / 1240$ where η is quantum efficiency, e is electron charge, h is plank's constant and c is the speed of light.[1, 17] For laser with λ = 640 nm, maximum R of 0.52 A W^{-1} can be achieved for η = 1 (100 % conversion). It can be seen from Figure 3d that responsivity values for all V_g's and P_{eff}'s are greater than 0.52 A W^{-1}, indicating gain larger than 1. Gain (G) can be estimated by $G = τ_m / τ_d$, where $τ_m$ is the minority carrier lifetime and $τ_d$ is the carrier drift or transit time.[1, 2] Trapping of minority carriers at traps states ($τ_m > τ_d$) leads to a gain larger than 1. Thus, photogating (local gating from trapped minority carriers) will result in a gain larger than 1. As seen the responsivity decreases as the effective laser intensity is increased, follows the relation $R ∝ (P_{eff})^{(γ-1)}$ (shown by the dashed line in Figure 3d) and it could be attributed to a decrease in the average carrier lifetime of minority charge carriers.[1] As light intensity increases, trap states gradually start filling up. At certain light intensities, all the trap states are filled and a further increase in intensity will result in the generation of minority carriers that cannot be trapped. As a result of this, $τ_m$ decreases thus reducing the gain and the responsivity.[1] It should be noted that at lower laser intensities (P_{eff} < 5 nW) and negative V_g's (-48 V and -36 V), responsivity remains constant due to the existence of sufficient number of unfilled trap states available for the minority charge carriers. In this case, responsivity follows the relation, $R = A_1/(A_2 + P_{eff})$ where A_1 and A_2 are fitting parameters.[39, 44] Saturation of responsivity at lower laser intensities have been observed in

graphene/PbS QDs[44] and graphene/MoS_2 phototransistors[39]. For our $ReSe_2$ phototransistor with V_g = 12 V (where photogating is dominant with γ ≈ 0.23), maximum responsivity of R ≈ 2618 AW^{-1} can be obtained at P_{eff} = 0.2 nW. Furthermore, R ≈ 2147 AW^{-1} can be obtained at P_{eff} = 0.2 nW and V_g = 0 V (γ ≈ 0.25). When gain > 1, quantum efficiency (η) is known as the external quantum efficiency (EQE) and is defined as EQE = R (h × c) / (e × λ) = R × 1240 / λ. EQE as a function P_{eff} in log-log scale for different applied gate voltages (-48 V < Vg < 60 V) is shown in Figure S3 of the supporting information. We found that EQE > 10^5 % for P_{eff} = 0.2 nW and V_g ≥ 0 V.

We further studied the photo-transport properties as a function of the temperature. Figure 4 depicts the results of photoconductivity of our $ReSe_2$ device at T = 140 K. The transport characterization at this temperature such as photogating effect, crossover between photoconductive and photogating effect (γ vs V_g), $I_{ph} ∝ (P_{eff})^γ$, $R ∝ (P_{eff})^{(γ-1)}$ etc. are similar to those measured at room temperature (Figure 3). The threshold gate voltage V_{th} can be seen shifting towards the positive gate voltage compared to the room temperature measurements presented in Figure 3a. This shift could be reasoned to electron needing higher energies to overcome a barrier induced by either stronger trapping of electron at localized/trap states or reduced tunnelling in thermionic emission process.[22] One striking differences is that, at V_g = 60 V, γ value → 0 (γ ≈ 0.05, Figure 4c), which is much lower than that at room temperature γ ≈ 0.25 (Figure 3c). This could be an indication of stronger trapping where the minority charge carries cannot escape from the trap states due to their lower thermal energy. This also results in R ≈ 1.6 × 10^4 AW^{-1} (Figure 4d) and EQE > 10^6 % (Supporting Information, figure S3).

To further illustrate the dependence on gate voltage and temperature on γ and R, we have plotted γ and R as a function of V_g and T in Figure 5. The variation of the power exponent (γ) as a function of applied gate voltage (V_g) for different temperatures (20 K < T < 300 K) is shown in Figure 5a. We found that in general, increasing the gate bias slowly drives the system from photo conductive to photo gated at any given

temperature. The photoconductive mechanism is strongest at low gate voltages and at higher temperatures. For example, as the applied gate voltage is increased from -48 V to 60 V, a switch from the photoconductive mechanism ($\gamma \rightarrow 1$) to the photogating mechanism ($\gamma < 1$) can be seen for all the temperatures studied (Figure 5a). Furthermore, an increase in the responsivity is also observed at higher V_g's as seen in Figure 5c. For the device shown, at gate voltages $V_g < 18$ V, lowering the temperature resulted in an increase in the value of the power exponent and consequently the decrese in the resposivity, as seen in Figures 5b and Figure 5d. For gate voltages $V_g > 18$ V, a contrasting result can be seen (Figure 5b and Figure 5d) as the photogating mechamism becomes stronger at lower temperatures resulting in higher responsivities. As the temperature is further reduced, photogating becomes slightly weaker as seen by a small increase in γ and a slight decrease in R.

Such behavior can be explained when considering the modulation of trapping/detrapping of minority carriers along with the movement of steady state Fermi level with varying temperature and gate voltages[45], as shown by the schematic in Figure 6a. For lower gate voltages, few minority carriers are trapped at room temperature and due to their thermal energy these carriers can be easily trapped/detrapped (lower right panel of Figure 6a). As temperatures decrease, steady state Fermi level moves closer to the valence band, resulting in a smaller number of trapped minority carriers (lower left panel of Figure 6a). Also, lower thermal energy translates into slower trapping and detrapping due to carrier freeze-out. At higher gate voltages, steady state Fermi level moves away from the valence band causing the number of states available for trapping/detrapping to increase, which result in a photogating dominated photocurrent (upper right panel of Figure 6a). Lowering the temperature will result in carrier freeze-out, resulting in strongly trapped charge carriers with stronger photogating effect (upper left panel of Figure 6a). As temperature is further reduced, steady state fermi level will shift towards the valence band thus lowering traps and slightly weaker photogating.

It has been reported that in the case of InSe,[17] the power exponent (γ), responsivity (R) and device response time (τ) follow a correlation such that $\tau \propto 1/\gamma$ (inversely proportional) and $\tau \propto R$ (linear dependence). This correlation is a consequence of photogating being the dominant mechanism in these phototransistors.[17] It should be noted that a competition between minority carrier lifetime (τ_m) and carrier drift or transit time (τ_d) plays a crucial role for this correlation. As carrier drift time depends on channel length, applied source drain voltage and mobility, τ_d remains constant upon variation of V_g and T. However, minority carrier lifetime (τ_m) is a function of V_g and T, as trapping and detrappping can be modulated by external factors such as temperature and gate voltages. For $\tau_m > \tau_d$, minority carries get trapped in long-lived traps thus resulting in slower response time as well as providing an external photogain which translates into higher responsivities. Also, $\gamma < 1$ is a consequence of processes such as trapping and carrier generation / recombination. By transitive property, we can conclude that responsivity should be inversely proportional to power exponent as $R \propto 1/\gamma$. Figure 6b shows a statistical plot of responsivity as a function of γ in logarithmic scale for various V_g's and T's for different effective intensities (0.2 nW < P_{eff} < 84.1 nW). A clear dependency of R on γ can be seen (denoted by a dashed line used to guide the eye), indicating an inverse proportionality between these two parameters. It should be noted that, for lower values of R (when $\gamma \rightarrow 1$) data points deviate from the dashed line, which could be attributed to a weak photogating, as discused for larger values of γ.[17]

Conclusions

In conclusion we have examined photoconductivity of few-layered ReSe$_2$ FET devices as a function of temperature. We observed high responsivity, R ~ 15,500 A/W and EQE ~ 3.2×10^6 % at T=140 K. Our investigations show that there is an intricate connection between the several fundamental processes that control the performance parameters of phototransistors. For example, a clear correlation between the photo-responsivity, R and power exponent γ, was observed. Broadly speaking; higher responsivities were found under conditions where the extracted γ values are significantly lower than unity or under photogating mechanism. This correlation between R and γ was found to be independent of either the operating temperature of the FET device or the applied gate voltage. Here we would like to emphasize that we have observed the variation of γ with temperature as well as gate voltage, where these parameters can modulate the trap states, but their effect on R is manifested through γ. Since it is generally believed that fractional values of γ (< 1) indicates a system where trap induced photogating is present, we can conclude that photogating phenomenon is responsible for such high values of responsivities that were observed in our devices. Although the study was specifically performed on ReSe$_2$ FETs, but we believe such correlation between R & γ will occur in any 2D photo FET as also evident from several recent studies.

Experimental Section

Growth of ReSe$_2$ Single Crystal:

ReSe$_2$ single crystals were synthesized through a traditional chemical vapor transport (CVT) method using iodine as the transport agent. The 99.999% pure Re and Se powders were both introduced into a clean quartz tube. The quartz tubes were clean using IPA, Acetone and at vacuum dried prior to loading the materials. The quartz tube was first evacuated and then heated to a temperature of 900 ^{0}C (at a heating rate of ~100 ^{0}C/h) and held at that temperature for 1 week. Subsequently, it was cooled to 850 ^{0}C at a rate of 10 ^{0}C/h, held for 6 hours, and subsequently quenched in air.

Fabrication of ReSe$_2$ Phototransistors:

Few layered flakes of ReSe$_2$ were exfoliated from the bulk single crystals by using scotch-tape and transferred onto highly p-doped Si wafers covered with a thermally evaporated 285 nm

thick layer of SiO_2. The electrical contacts were fabricated using a Lesker PVD 250 electron beam evaporator and consisted of 80 nm Au onto a 5 nm Cr film. Contacts were patterned using a laser-writer (Model # LW405). After gold evaporation, the devices were annealed at 300 ^{0}C for ~ 3h in an Ar environment to remove any unwanted remaining photoresist from the top of the channel. Atomic force microscopy imaging was performed to verify the thickness of the $ReSe_2$ crystal. After the deposition of metal contacts the wafer was transferred onto a chip holder (Spectrum Semiconductor, CSB02842) and glued using silver paste. Cr/Au contacts were connected to the chip holder by wire bonding using Au wire. These devices were further annealed at 150 ^{0}C under Argon atmosphere (50 sccm) for 2 hours to remove any moisture and clean the surface of the channel.

Characterization of ReSe$_2$ Phototransistors:

For opto-electronic studies, the chip holder was mounted onto cold head of cryostat (SHI Cryogenics Group, RDK-101D). Cold head chamber was evacuated using a turbo pump (BOC Edwards) to high vacuum (~ 10^5 torr). The channel of the devices (4.5 μm × 6 μm) were illuminated by a continuous laser (Coherent Inc., CUBE 640-40C) of wavelength λ = 640 nm (E = 1.94 eV) with a spot size of ~ 3 mm in diameter and tunable laser intensity (0.85 mW ≤ P ≤ 40 mW) through an optical window. In our experiment the size of our laser spot is significantly larger than the device geometry.

Author Contributions

S.T. supervised and designed the experiments. P.D.P., M.W., R.A. and L.W. performed the electronic and optoelectronic transport experiments. P.D.P performed the data analysis. P.D.P and S.T. came up with the conclusions and drafted the first version of the manuscript. D.R. and L.B. synthesized $ReSe_2$ crystals. K.K.R, B.C., D.R., R.D., A.S. and N.P fabricated $ReSe_2$ devices. All authors contributed to the final version of the manuscript.

Conflicts of interest

There are no conflicts to declare.

Acknowledgements

Notes and references

1. H. Fang and W. Hu, *Advanced Science*, 2017, **4**, 1700323.
2. M. Buscema, J. O. Island, D. J. Groenendijk, S. I. Blanter, G. A. Steele, H. S. J. van der Zant and A. Castellanos-Gomez, *Chemical Society Reviews*, 2015, **44**, 3691-3718.
3. K. Khan, A. K. Tareen, M. Aslam, R. Wang, Y. Zhang, A. Mahmood, Z. Ouyang, H. Zhang and Z. Guo, *Journal of Materials Chemistry C*, 2020, **8**, 387-440.
4. B. Wang, S. Zhong, P. Xu and H. Zhang, *Journal of Materials Chemistry C*, 2020, **8**, 15526-15574.
5. M. Wasala, H. I. Sirikumara, Y. Raj Sapkota, S. Hofer, D. Mazumdar, T. Jayasekera and S. Talapatra, *Journal of Materials Chemistry C*, 2017, **5**, 11214-11225.
6. F. Zhou, J. Chen, X. Tao, X. Wang and Y. Chai, *Research*, 2019, **2019**, 9490413.
7. M. Mohl, A.-R. Rautio, G. A. Asres, M. Wasala, P. D. Patil, S. Talapatra and K. Kordas, *Advanced Materials Interfaces*, 2020, **7**, 2000002.
8. N. R. Pradhan, R. Thantirige, P. D. Patil, S. A. McGill and S. Talapatra, in *2D Nanoscale Heterostructured Materials : Synthesis, Properties, and Applications*, eds. S. Jit and S. Das, Elsevier, Amsterdam, Netherlands, 2020, ch. 6, pp. 151-194.
9. J. O. Island, S. I. Blanter, M. Buscema, H. S. J. van der Zant and A. Castellanos-Gomez, *Nano Letters*, 2015, **15**, 7853-7858.
10. S. Ghosh, P. D. Patil, M. Wasala, S. Lei, A. Nolander, P. Sivakumar, R. Vajtai, P. Ajayan and S. Talapatra, *2D Materials*, 2017, **5**, 015001.
11. S. Ghosh, M. Wasala, N. R. Pradhan, D. Rhodes, P. D. Patil, M. Fralaide, Y. Xin, S. A. McGill, L. Balicas and S. Talapatra, *Nanotechnology*, 2018, **29**, 484002.
12. C. Garcia, N. R. Pradhan, D. Rhodes, L. Balicas and S. A. McGill, *Journal of Applied Physics*, 2018, **124**, 204306.
13. J. Miao and F. Zhang, *Journal of Materials Chemistry C*, 2019, **7**, 1741-1791.
14. M. S. Marcus, J. M. Simmons, O. M. Castellini, R. J. Hamers and M. A. Eriksson, *Journal of Applied Physics*, 2006, **100**, 084306.
15. X. Guo, W. Wang, H. Nan, Y. Yu, J. Jiang, W. Zhao, J. Li, Z. Zafar, N. Xiang, Z. Ni, W. Hu, Y. You and Z. Ni, *Optica*, 2016, **3**, 1066-1070.
16. H. Lee, J. Ahn, S. Im, J. Kim and W. Choi, *Scientific Reports*, 2018, **8**, 11545.
17. Q. Zhao, W. Wang, F. Carrascoso-Plana, W. Jie, T. Wang, A. Castellanos-Gomez and R. Frisenda, *Materials Horizons*, 2020, **7**, 252-262.
18. M. Hafeez, L. Gan, A. Saleem Bhatti and T. Zhai, *Materials Chemistry Frontiers*, 2017, **1**, 1917-1932.
19. C. Gong, Y. Zhang, W. Chen, J. Chu, T. Lei, J. Pu, L. Dai, C. Wu, Y. Cheng, T. Zhai, L. Li and J. Xiong, *Advanced Science*, 2017, **4**, 1700231.
20. E. Liu, Y. Fu, Y. Wang, Y. Feng, H. Liu, X. Wan, W. Zhou, B. Wang, L. Shao, C.-H. Ho, Y.-S. Huang, Z. Cao, L. Wang, A. Li, J. Zeng, F. Song, X. Wang, Y. Shi, H. Yuan, H. Y. Hwang, Y. Cui, F. Miao and D. Xing, *Nature Communications*, 2015, **6**, 6991.

21. E. Liu, M. Long, J. Zeng, W. Luo, Y. Wang, Y. Pan, W. Zhou, B. Wang, W. Hu, Z. Ni, Y. You, X. Zhang, S. Qin, Y. Shi, K. Watanabe, T. Taniguchi, H. Yuan, H. Y. Hwang, Y. Cui, F. Miao and D. Xing, *Advanced Functional Materials*, 2016, **26**, 1938-1944.

22. N. R. Pradhan, C. Garcia, B. Isenberg, D. Rhodes, S. Feng, S. Memaran, Y. Xin, A. McCreary, A. R. H. Walker, A. Raeliarijaona, H. Terrones, M. Terrones, S. McGill and L. Balicas, *Scientific Reports*, 2018, **8**, 12745.

23. S.-H. Jo, H. W. Lee, J. Shim, K. Heo, M. Kim, Y. J. Song and J.-H. Park, *Advanced Science*, 2018, **5**, 1700423.

24. E. Zhang, P. Wang, Z. Li, H. Wang, C. Song, C. Huang, Z.-G. Chen, L. Yang, K. Zhang, S. Lu, W. Wang, S. Liu, H. Fang, X. Zhou, H. Yan, J. Zou, X. Wan, P. Zhou, W. Hu and F. Xiu, *ACS Nano*, 2016, **10**, 8067-8077.

25. K.-C. Lee, S.-H. Yang, Y.-S. Sung, Y.-M. Chang, C.-Y. Lin, F.-S. Yang, M. Li, K. Watanabe, T. Taniguchi, C.-H. Ho, C.-H. Lien and Y.-F. Lin, *Advanced Functional Materials*, 2019, **29**, 1809011.

26. W. L. Kalb and B. Batlogg, *Physical Review B*, 2010, **81**, 035327.

27. K. K. Ng and S. M. Sze, *Physics of Semiconductor Devices 3rd Edition*, John Wiley & Sons Incorporated, 2006.

28. P. D. Patil, S. Ghosh, M. Wasala, S. Lei, R. Vajtai, P. M. Ajayan, A. Ghosh and S. Talapatra, *ACS Nano*, 2019, **13**, 13413-13420.

29. M. Wasala, P. D. Patil, S. Ghosh, R. Alkhaldi, L. Weber, S. Lei, R. Vajtai, P. M. Ajayan and S. Talapatra, *2D Materials*, 2020, **7**, 025030.

30. P. D. Patil, S. Ghosh, M. Wasala, S. Lei, R. Vajtai, P. M. Ajayan and S. Talapatra, *Electronics*, 2019, **8**, 645.

31. J. Hong, Z. Hu, M. Probert, K. Li, D. Lv, X. Yang, L. Gu, N. Mao, Q. Feng, L. Xie, J. Zhang, D. Wu, Z. Zhang, C. Jin, W. Ji, X. Zhang, J. Yuan and Z. Zhang, *Nature Communications*, 2015, **6**, 6293.

32. S. Ghatak, A. N. Pal and A. Ghosh, *ACS Nano*, 2011, **5**, 7707-7712.

33. H. Kim, D. Kim, C. Jeong, J. Lee and H. Kwon, *IEEE Electron Device Letters*, 2017, **38**, 481-484.

34. N. Haratipour, S. Namgung, S.-H. Oh and S. J. Koester, *ACS Nano*, 2016, **10**, 3791-3800.

35. S. Kim, A. Konar, W.-S. Hwang, J. H. Lee, J. Lee, J. Yang, C. Jung, H. Kim, J.-B. Yoo, J.-Y. Choi, Y. W. Jin, S. Y. Lee, D. Jena, W. Choi and K. Kim, *Nature Communications*, 2012, **3**, 1011.

36. S.-L. Li, K. Tsukagoshi, E. Orgiu and P. Samorì, *Chemical Society Reviews*, 2016, **45**, 118-151.

37. G. Ghibaudo, *Electronics Letters*, 1988, **24**, 543-545.

38. H.-Y. Chang, W. Zhu and D. Akinwande, *Applied Physics Letters*, 2014, **104**, 113504.

39. K. Roy, M. Padmanabhan, S. Goswami, T. P. Sai, G. Ramalingam, S. Raghavan and A. Ghosh, *Nature Nanotechnology*, 2013, **8**, 826-830.

40. Z. Yu, Z.-Y. Ong, S. Li, J.-B. Xu, G. Zhang, Y.-W. Zhang, Y. Shi and X. Wang, *Advanced Functional Materials*, 2017, **27**, 1604093.

41. N. F. Mott and E. A. Davis, *Electronic processes in non-crystalline materials*, Clarendon Press ; Oxford University Press, Oxford; New York, 1979.

42. M. M. Furchi, D. K. Polyushkin, A. Pospischil and T. Mueller, *Nano Letters*, 2014, **14**, 6165-6170.

43. B. Miller, E. Parzinger, A. Vernickel, A. W. Holleitner and U. Wurstbauer, *Applied Physics Letters*, 2015, **106**, 122103.

44. G. Konstantatos, M. Badioli, L. Gaudreau, J. Osmond, M. Bernechea, F. P. G. de Arquer, F. Gatti and F. H. L. Koppens, *Nature Nanotechnology*, 2012, **7**, 363-368.

45. A. Rose, *Physical Review*, 1955, **97**, 322-333.